PCCP

COMMUNICATION

View Article Online
View Journal | View Issue

Cite this: *Phys. Chem. Chem. Phys.*, 2019, **21**, 8201

Received 15th March 2019,
Accepted 1st April 2019

DOI: 10.1039/c9cp01474h

rsc.li/pccp

Detailed electronic structure of a high-spin cobalt(II) complex determined from NMR and THz-EPR spectroscopy†

Alexander A. Pavlov,*[ab] Joscha Nehrkorn,[cd] Yanina A. Pankratova,[ae] Mykhaylo Ozerov,[c] Elena A. Mikhalyova,[f] Alexander V. Polezhaev,[ag] Yulia V. Nelyubina[ab] and Valentin V. Novikov[ab]

Here we report a combined use of THz-EPR and NMR spectroscopy for obtaining a detailed electronic structure of a long-known high-spin complex, cobalt(II) bis[tris(pyrazolyl)borate]. The lowest inter-Kramers transition was directly measured by THz-EPR spectroscopy, while the energies of higher Kramers doublets were estimated by a recently proposed NMR-based approach. Together, they produced magnetic parameters for a full model that explicitly includes spin–orbit coupling. This approach is applicable to all transition metal ions for which the spin–orbit coupling cannot be treated perturbatively.

Getting insight into the fine details of electronic structure is crucial for rational design of new magnetic materials based on transition metal complexes, such as single molecule magnets[1–4] and spin-crossover compounds[5–7] in molecular spintronics[8,9] or paramagnetic tags in structural biology.[10–12] Many methods exist to probe the electronic structure of their ground term, which governs the magnetic properties of these materials. In addition to commonly employed techniques, such as optical absorption and fluorescence spectroscopy,[13,14] EPR spectroscopy,[15] magnetometry[16,17] and X-ray diffraction,[18] other approaches are being developed. Among them, frequency-domain Fourier-transform THz electron paramagnetic resonance spectroscopy (THz-EPR) directly probes transitions within an exceptionally broad excitation range (up to hundreds cm^{-1}), far beyond the range of routine EPR spectrometers.[19,20] Although it provides unique information on the electronic structure of transition metal complexes, accessing higher lying excited states is still a challenge due to the selection rules and low temperatures usually employed in these measurements to obtain better signal-to-noise ratios. Therefore, a technique complimentary to THz-EPR spectroscopy is needed, such as, *e.g.*, NMR spectroscopy. A popular tool for identifying diamagnetic compounds in solutions, it recently emerged as a powerful approach for probing the electronic structure of paramagnetic transition metal complexes at ambient temperatures.[21–28] Nevertheless, neither THz-EPR nor paramagnetic NMR spectroscopy are routinely used for this purpose. Here, both of them are applied to obtain the detailed electronic structure of a high-spin (HS) cobalt(II) complex with a trigonal antiprismatic geometry, which, *e.g.*, often accounts for single molecule magnet behaviour.[29] A well-known example of such type of complexes is cobalt(II) bis[tris(pyrazolyl)borate] (**$CoTp_2$**), introduced by S. Trofimenko in 1966.[30] Its electronic structure has already been probed by a variety of optical and magnetic resonance methods.[31–35] They showed that strong spin–orbit coupling (SOC) split the $^4T_{1g}$ ground term of the cobalt(II) ion in a trigonal antiprismatic D_3 environment into six Kramers doublets (KDs), and the four lowest KDs are almost equidistant in energy with a separation of 206–242 cm^{-1} (Fig. 1).[32]

We collected the THz-EPR spectra (see ESI† for experimental details) of **$CoTp_2$** from its fine-crystalline sample at NHMFL (Tallahassee, FL). Subsequently constructed Magnetic Field Division spectra (MDS) have very sharp features that are rarely observed in these kind of spectra.[36,37] In the obtained MDS (see ref. 19 for more details), a minimum appears at 197 cm^{-1} in the zero magnetic field (Fig. 2) together with maxima at lower and higher energies, respectively. Upon increasing the magnetic field, the former feature broadens, and the latter shifts to lower and higher energies, respectively. While the minimum and the low-energy maximum broaden beyond recognition at higher

[a] *A.N.Nesmeyanov Institute of Organoelement Compounds, Russian Academy of Sciences, Vavilova str. 28, 119991, Moscow, Russia. E-mail: pavlov@ineos.ac.ru*
[b] *Moscow Institute of Physics and Technology, Institutskiy per., 9, Dolgoprudny, Moscow Region, 141701, Russian Federation*
[c] *National High Magnetic Field Laboratory & Florida State University, 1800 E. Paul Dirac Drive, Tallahassee, FL 32310-3706, USA*
[d] *Max Planck Institute for Chemical Energy Conversion, Stiftstr. 34–36, 45470 Mülheim an der Ruhr, Germany*
[e] *Lomonosov Moscow State University, Leninskie Gory, Moscow, 119991, Russia*
[f] *L.V.Pisarzhevskii Institute of Physical Chemistry of the National Academy of Sciences of the Ukraine, Prospekt Nauki 31, Kiev, 03028, Ukraine*
[g] *Bauman Moscow State Technical University, 2-Ya Baumanskaya Ulitsa 5, Moscow, 105005, Russia*

† Electronic supplementary information (ESI) available: Experimental and calculation details as well as supplementary tables and figures. See DOI: 10.1039/c9cp01474h

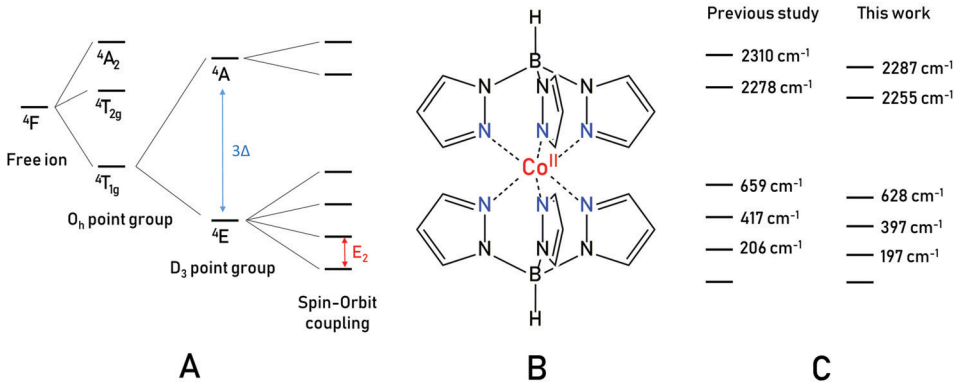

Fig. 1 (A) Electronic structure of the high-spin cobalt(II) ion in a D_3 environment with significant spin–orbit coupling. Δ is a parameter of crystal field splitting of the ground term $^4T_{1g}$. (B) Cobalt(II) bis[tris(pyrazolyl)borate] **CoTp$_2$**. (C) Energy levels in **CoTp$_2$** according to the previous study[32] and in this work.

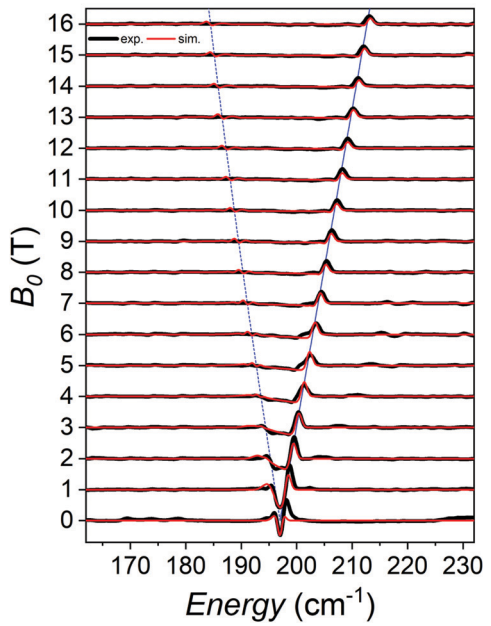

Fig. 2 THz-EPR spectra for a fine-crystalline sample of **CoTp$_2$** at 4.2 K (black). MDS spectra at the magnetic field B_0 are obtained by dividing a spectrum measured at B_0 by a spectrum measured at B_0 + 1 T; data is offset for B_0. Simulation with the spin-Hamiltonian (1) (S = 3/2, D = −98.5 cm^{-1}, $g_\perp$ = 1.9, $g_\parallel$ = 2.1) is shown in red. Blue lines correspond to the transition energies for B_0 perpendicular (dashed) and parallel (solid) to the molecular easy axis.

fields, the high-energy maximum is recognizable over the probed field range. No further magnetic signals could be detected.

The simulations of FD-FT THz-EPR MDS with an effective spin-Hamiltonian (1), which has no rhombic terms due to the axial symmetry of **CoTp$_2$**, gave us the magnitude of the zero-field splitting (ZFS) parameter $|D|$ of 98.5 cm^{-1} and $g_\perp$ = 1.9, $g_\parallel$ = 2.1.[38–40]

$$\hat{\mathcal{H}} = D\left(\hat{\boldsymbol{S}}_z^2 - \frac{\hat{\boldsymbol{S}}^2}{3}\right) + \mu_B \boldsymbol{B}_0 \cdot \mathrm{diag}(g_\perp, g_\perp, g_\parallel) \cdot \hat{\boldsymbol{S}} \qquad (1)$$

Although the effective spin Hamiltonian should not be, in fact, used for systems with low-lying orbital states,[32] simulations with eqn (1) provided spectra that agree nicely with those measured experimentally (see Fig. 2), as they were measured at 4.2 K. At this temperature, only the 1st KD is significantly populated in **CoTp$_2$**; probabilities of transitions from the 1st KD to the 3rd and higher lying KDs are hardly probable, so they cannot be accessed with THz-EPR spectroscopy. However, it might be still possible with techniques operating at higher temperatures, such as NMR spectroscopy. In an approach that we have recently proposed,[21,22,41] the energy of the KDs are related to the molar magnetic susceptibility tensor anisotropy $\Delta\chi$, which can be obtained by the NMR spectroscopy:

$$\Delta\chi_{ax} = \chi_\parallel - \chi_\perp \qquad (2)$$

$$\chi_a = \frac{N_A kT}{10}\frac{\partial^2}{\partial B_a^2}\ln\left(\sum_i e^{-\frac{\langle\psi_i|\hat{\mathcal{H}}|\psi_i\rangle}{kT}}\right) \qquad (3)$$

where ψ_i are the eigenvectors of a spin-Hamiltonian; $a = \parallel, \perp$.

In the NMR spectra recorded from a solution of a paramagnetic compound (Fig. S1–S3, ESI†), this anisotropy $\Delta\chi$ causes a pseudocontact chemical shift of each nucleus, δ_{PCS}, according to where it is found related to the paramagnetic center in a molecule. In the case of an axial symmetry, such as in **CoTp$_2$**:

$$\delta_{PCS} = \frac{1}{12\pi r^3}\Delta\chi_{ax}(3\cos^2\theta - 1) \qquad (4)$$

Here, $\Delta\chi_{ax}$ is the axial anisotropy of the magnetic susceptibility tensor (χ-tensor), and r and θ are polar coordinates of a nucleus in the χ-tensor frame.

The other two components of the chemical shifts in the NMR spectra are of diamagnetic and contact origins. The diamagnetic contribution, which arises from the shielding of nuclei by the orbital motion of paired electrons, can easily be obtained by NMR spectroscopy of a diamagnetic analogue, such as an isostructural complex of a diamagnetic metal or a free ligand. The contact contribution δ_{CS} results from the delocalization of spin density ρ through a system of molecular orbitals

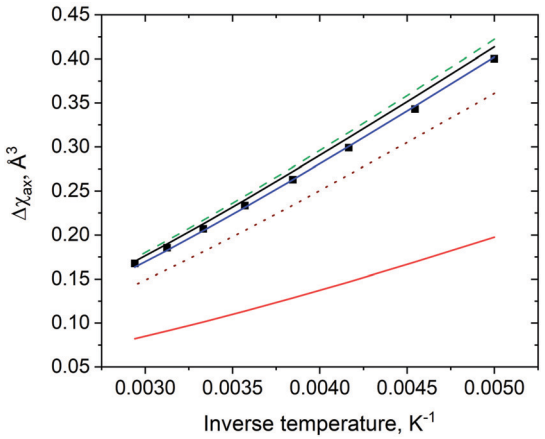

Fig. 3 Temperature dependence of the magnetic susceptibility tensor anisotropy $\Delta\chi_{ax}$ for a solution of **CoTp$_2$** in toluene-d$_8$ (black squares). Various simulations are included as lines. Simulations using eqn (1) and D = −98.5 cm^{-1}, $g_\perp$ = 1.9, $g_\parallel$ = 2.1 are shown as red solid line. Further simulations were done with eqn (6). Simulation using the parameters (λ = 152.4 cm^{-1}, σ = 1.366, Δ = −632 cm^{-1}) based on previous results[32] are shown as black solid line. The best fit (λ = 147.3 cm^{-1}, σ = 1.350 and Δ = −632 cm^{-1}) is shown as blue solid line. To visualize the sensitivity to Δ, we included simulations with fixed Δ values of −900 cm^{-1} (dashed green line) and −400 cm^{-1} (doted brown line).

and is, therefore, accessible by a simple quantum chemical calculation:

$$\delta_{CS} = \frac{4\pi\mu_B^2}{9kT} g^{iso} \rho \qquad (5)$$

For **CoTp$_2$**, the introduced approach (see ESI† for more details) allowed us to obtain chemical shifts in ^{1}H, ^{13}C and ^{11}B NMR spectra that were in a good agreement with those measured experimentally from its solution in toluene-d$_8$ at 200–340 K (Fig. S4–S12, ESI†). The fit between the calculated and measured chemical shifts, which is at the core of this procedure, produced accurate values of the anisotropy $\Delta\chi_{ax}$ in the corresponding temperature range (Fig. 3). They were then simulated using various models.

For most transition metal ions, the SOC can be treated as a perturbation leading to the ZFS formalism shown in eqn (1).[42] An exception is HS Co(II) ion in a (distorted) octahedral or trigonal antiprismatic environment. To model the magnetic properties of **CoTp$_2$**, SOC has to be explicitly included. If the common $^4T_{1g} \rightarrow {}^4P$ isomorphism is used,[43] an effective orbital angular momentum L is 1, and the Hamiltonian takes the following form:

$$\hat{\mathcal{H}} = \sigma\lambda\hat{L}\cdot\hat{S} + \Delta\left(3\hat{L}_z^2 - \hat{L}^2\right) + \mu_B B_0\left(-\sigma\hat{L} + g_e\hat{S}\right) \qquad (6)$$

Here, λ is the SOC parameter, σ is an orbital reduction factor and Δ parametrizes the crystal field splitting of the ground term $^4T_{1g}$ (Fig. 1), g_e is the free electron g-factor. A known limitation of this model is the interdependency of the above magnetic parameters. Although it is regularly applied to fit magnetometry results, obtaining a unique set of parameters with it is quite challenging. Thus, additional methods are required for this purpose.

While the results from THz-EPR spectroscopy could also be described with the effective spin Hamiltonian (eqn (1)), we failed to obtain reasonable convergence to the NMR data. Therefore, the more elaborate Hamiltonian given in eqn (6) was used. In the fitting routine, the zero-field energy difference between the first and second KD (E_2) was fixed to the spectroscopic value of 197 cm^{-1}. The resulting values λ = 147.3 cm^{-1}, σ = 1.350 and Δ = −632 cm^{-1} allowed reproducing the experimental THz-EPR spectra (Fig. S13, ESI†) and the magnetic susceptibility for a solution of **CoTp$_2$** (Fig. S14, ESI†). Parameters based on the previously published energy diagram[32] (λ = 152.4 cm^{-1}, σ = 1.366, Δ = −632 cm^{-1}) resulted in a slightly worse agreement with the NMR data (see Fig. 3) but the THz-EPR spectra were not reproduced at all (Fig. S15, ESI†). Our results indicate that the prefactor $|\sigma\cdot\lambda|$ of the SOC is almost equal to E_2. Numerical calculations (Fig. S17, ESI†) showed that this is the case for $|\Delta| \gg |\sigma\cdot\lambda|$, so that $|\Delta| > 3|\sigma\cdot\lambda|$ as obtained here is sufficient to reach this limit. It is reasonable to assume that THz-EPR spectroscopy is less sensitive to higher-lying levels than paramagnetic NMR spectroscopy. Therefore, the effective spin Hamiltonian (eqn (1)) could be applied for the former but not for the latter.

The combination of THz-EPR and paramagnetic NMR spectroscopies thus gave very accurate magnetic parameters and, as a result, a detailed picture of the energy splitting in the $^4T_{1g}$ state of the complex **CoTp$_2$** (Table S1, ESI†). Although here it was used for the HS Co(II) ion in a trigonal antiprismatic environment, this approach might be applicable to other complexes containing transition metal ions for which SOC have to be considered explicitly.

In conclusion, a detailed electronic structure is derived for the long-known cobalt(II) bis[tris(pyrazolyl)borate] by the direct observation of the lowest inter-Kramers transition in its THz-EPR spectra and by use of an NMR-based approach to obtaining the energies of higher lying KDs.

Such insights are essentially needed for all the paramagnetic ions with a significant contribution from SOC, including lanthanides and some transition metals. For them, the effective spin Hamiltonian is no longer valid, and an appropriate Hamiltonian with individual SOC and crystal field terms have to be used. The methods to obtain its often elusive parameters by NMR spectroscopy are especially attractive, as such experiments are relatively fast and cheap and, therefore, allow for high-throughput assessing of new transition metal complexes as potential materials in molecular spintronics and structural biology.

Conflicts of interest

There are no conflicts to declare.

Acknowledgements

This study was financially supported by Russian Science Foundation (project no. 18-73-00113). THz-EPR experiments were performed at the National High Magnetic Field Laboratory,

which is supported by National Science Foundation Cooperative Agreement No. DMR-1644779 and the State of Florida. Y. V. N. and E. A. M. acknowledge the Foundation Volkswagen Stiftung Trilateral Partnerships – Cooperation Projects between Scholars and Scientists from Ukraine, Russia and Germany, Ref. number 90343. Chemical characterization was performed with the financial support from Ministry of Science and Higher Education of the Russian Federation using the equipment of the Center for Molecular Composition Studies of INEOS RAS.

Notes and references

1 R. Sessoli, D. Gatteschi, A. Caneschi and M. Novak, *Nature*, 1993, **365**, 141.
2 R. Sessoli and A. K. Powell, *Coord. Chem. Rev.*, 2009, **253**, 2328–2341.
3 J. M. Frost, K. L. Harriman and M. Murugesu, *Chem. Sci.*, 2016, **7**, 2470–2491.
4 M. Atanasov, D. Aravena, E. Suturina, E. Bill, D. Maganas and F. Neese, *Coord. Chem. Rev.*, 2015, **289**, 177–214.
5 J. F. Létard, G. Chastanet, P. Guionneau and C. Desplanches, *Spin-Crossover Materials: Properties and Applications*, 2013, pp. 475–506.
6 G. Molnár, S. Rat, L. Salmon, W. Nicolazzi and A. Bousseksou, *Adv. Mater.*, 2018, **30**, 1703862.
7 K. S. Kumar and M. Ruben, *Coord. Chem. Rev.*, 2017, **346**, 176–205.
8 R. E. Winpenny, *Angew. Chem., Int. Ed.*, 2008, **47**, 7992–7994.
9 L. Bogani and W. Wernsdorfer, *Nanoscience And Technology: A Collection of Reviews from Nature Journals*, World Scientific, 2010, pp. 194–201.
10 I. Bertini, C. Luchinat, G. Parigi and E. Ravera, *NMR of Paramagnetic Molecules: Applications to Metallobiomolecules and Models*, Elsevier, 2016.
11 H. Yagi, K. B. Pilla, A. Maleckis, B. Graham, T. Huber and G. Otting, *Structure*, 2013, **21**, 883–890.
12 M. A. Hass and M. Ubbink, *Curr. Opin. Struct. Biol.*, 2014, **24**, 45–53.
13 S. L. Reddy, T. Endo and G. S. Reddy,*Advanced Aspects of Spectroscopy*, InTech, 2012.
14 Y. Chia and M. Tay, *Dalton Trans.*, 2014, **43**, 13159–13168.
15 *Electron Paramagnetic Resonance*, ed. B. Gilbert, Royal Society of Chemistry, 2008, vol. 21.
16 D. N. Woodruff, R. E. Winpenny and R. A. Layfield, *Chem. Rev.*, 2013, **113**, 5110–5148.
17 D. Gatteschi, R. Sessoli and J. Villain, *Molecular nanomagnets*, Oxford University Press on Demand, 2006.
18 C. Gatti and P. Macchi, *Modern charge-density analysis*, Springer Science & Business Media, 2012.
19 J. Nehrkorn, K. Holldack, R. Bittl and A. Schnegg, *J. Magn. Reson.*, 2017, **280**, 10–19.
20 P. Neugebauer, D. Bloos, R. Marx, P. Lutz, M. Kern, D. Aguilà, J. Vaverka, O. Laguta, C. Dietrich and R. Clérac, *Phys. Chem. Chem. Phys.*, 2018, **20**, 15528–15534.
21 A. A. Pavlov, G. L. Denisov, M. A. Kiskin, Y. V. Nelyubina and V. V. Novikov, *Inorg. Chem.*, 2017, **56**, 14759–14762.
22 V. V. Novikov, A. A. Pavlov, Y. V. Nelyubina, M.-E. Boulon, O. A. Varzatskii, Y. Z. Voloshin and R. E. Winpenny, *J. Am. Chem. Soc.*, 2015, **137**, 9792–9795.
23 T. Morita, M. Damjanovic, K. Katoh, Y. Kitagawa, N. Yasuda, Y. Lan, W. Wernsdorfer, B. K. Breedlove, M. Enders and M. Yamashita, *J. Am. Chem. Soc.*, 2018, **140**, 2995–3007.
24 M. Hiller, S. Krieg, N. Ishikawa and M. Enders, *Inorg. Chem.*, 2017, **56**, 15285–15294.
25 M. Findeisen, T. Brand and S. Berger, *Magn. Reson. Chem.*, 2007, **45**, 175–178.
26 M. Damjanovic, K. Katoh, M. Yamashita and M. Enders, *J. Am. Chem. Soc.*, 2013, **135**, 14349–14358.
27 V. V. Novikov, A. A. Pavlov, A. S. Belov, A. V. Vologzhanina, A. Savitsky and Y. Z. Voloshin, *J. Phys. Chem. Lett.*, 2014, **5**, 3799–3803.
28 A. A. Pavlov, Y. V. Nelyubina, S. V. Kats, L. V. Penkova, N. N. Efimov, A. O. Dmitrienko, A. V. Vologzhanina, A. S. Belov, Y. Z. Voloshin and V. V. Novikov, *J. Phys. Chem. Lett.*, 2016, **7**, 4111–4116.
29 J. Zhang, J. Li, L. Yang, C. Yuan, Y.-Q. Zhang and Y. Song, *Inorg. Chem.*, 2018, **57**, 3903–3912.
30 S. Trofimenko, *J. Am. Chem. Soc.*, 1966, **88**, 1842–1844.
31 S. Trofimenko, *J. Am. Chem. Soc.*, 1967, **89**, 3170–3177.
32 J. Jesson, *J. Chem. Phys.*, 1966, **45**, 1049–1056.
33 J. Jesson, S. Trofimenko and D. Eaton, *J. Am. Chem. Soc.*, 1967, **89**, 3148–3158.
34 D. L. Tierney, *J. Phys. Chem. A*, 2012, **116**, 10959–10972.
35 A. R. Marts, J. C. Kaine, R. R. Baum, V. L. Clayton, J. R. Bennett, L. J. Cordonnier, R. McCarrick, A. Hasheminasab, L. A. Crandall and C. J. Ziegler, *Inorg. Chem.*, 2016, **56**, 618–626.
36 M. A. Palacios, J. Nehrkorn, E. A. Suturina, E. Ruiz, S. Gómez-Coca, K. Holldack, A. Schnegg, J. Krzystek, J. M. Moreno and E. Colacio, *Chem. – Eur. J.*, 2017, **23**, 11649–11661.
37 J. Nehrkorn, S. L. Veber, L. A. Zhukas, V. V. Novikov, Y. V. Nelyubina, Y. Z. Voloshin, K. Holldack, S. Stoll and A. Schnegg, *Inorg. Chem.*, 2018, **57**, 15330–15340.
38 S. Stoll and A. Schweiger, *J. Magn. Reson.*, 2006, **178**, 42–55.
39 J. Nehrkorn, J. Telser, K. Holldack, S. Stoll and A. Schnegg, *J. Phys. Chem. B*, 2015, **119**, 13816–13824.
40 J. Nehrkorn, A. Schnegg, K. Holldack and S. Stoll, *Phys. Rev. Lett.*, 2015, **114**, 010801.
41 A. A. Pavlov, S. A. Savkina, A. S. Belov, Y. Z. Voloshin, Y. V. Nelyubina and V. V. Novikov, *ACS Omega*, 2018, **3**, 4941–4946.
42 A. Abragam and B. Bleaney, *Electron paramagnetic resonance of transition ions*, OUP, Oxford, 2012.
43 M. Lines, *J. Chem. Phys.*, 1971, **55**, 2977–2984.

